Downloaded from jnm.snmjournals.org by UCL Library Services on July 9, 2019. For personal use only.

Flutriciclamide (^{18}F-GE180) PET: First-in-Human PET Study of Novel Third-Generation In Vivo Marker of Human Translocator Protein

Zhen Fan*[1], Valeria Calsolaro*[1], Rebecca A. Atkinson[1], Grazia D. Femminella[1], Adam Waldman[1], Christopher Buckley[2], William Trigg[2], David J. Brooks[1,3], Rainer Hinz[4], and Paul Edison[1]

[1]Neurology Imaging Unit, Imperial College London, Hammersmith Hospital, London, United Kingdom; [2]GE Healthcare, Grove Centre, Amersham, United Kingdom; [3]Institute of Clinical Medicine, Aarhus University, Aarhus, Denmark; and [4]Wolfson Molecular Imaging Centre, University of Manchester, Manchester, United Kingdom

Neuroinflammation is associated with neurodegenerative disease. PET radioligands targeting the 18-kDa translocator protein (TSPO) have been used as in vivo markers of neuroinflammation, but there is an urgent need for novel probes with improved signal-to-noise ratio. Flutriciclamide (^{18}F-GE180) is a recently developed third-generation TSPO ligand. In this first study, we evaluated the optimum scan duration and kinetic modeling strategies for ^{18}F-GE180 PET in (older) healthy controls. **Methods**: Ten healthy controls, 6 TSPO high-affinity binders, and 4 mixed-affinity binders were recruited. All subjects underwent detailed neuropsychologic tests, MRI, and a 210-min ^{18}F-GE180 dynamic PET/CT scan using metabolite-corrected arterial plasma input function. We evaluated 5 different kinetic models: irreversible and reversible 2-tissue-compartment models, a reversible 1-tissue model, and 2 models with an extra irreversible vascular compartment. The minimal scan duration was established using 210-min scan data. The feasibility of generating parametric maps was also investigated using graphical analysis. **Results:** ^{18}F-GE180 concentration was higher in plasma than in whole blood during the entire scan duration. The volume of distribution (V_T) was 0.17 in high-affinity binders and 0.12 in mixed-affinity binders using the kinetic model. The model that best represented brain ^{18}F-GE180 kinetics across regions was the reversible 2-tissue-compartment model (2TCM4k), and 90 min resulted as the optimum scan length required to obtain stable estimates. Logan graphical analysis with arterial input function gave a V_T highly consistent with V_T in the kinetic model, which could be used for voxelwise analysis. **Conclusion:** We report for the first time, to our knowledge, the kinetic properties of the novel third-generation TSPO PET ligand ^{18}F-GE180 in humans: 2TCM4k is the optimal method to quantify the brain uptake, 90 min is the optimal scan length, and the Logan approach could be used to generate parametric maps. Although these control subjects have shown relatively low V_T, the methodology presented here forms the basis for quantification for future PET studies using ^{18}F-GE180 in different pathologies.

Key Words: GE180; flutriciclamide; kinetic model; Logan analysis; PET

J Nucl Med 2016; 57:1753–1759
DOI: 10.2967/jnumed.115.169078

Microglia play a crucial role as the first line of defense when neuronal damage occurs. Under normal conditions, microglial cells are in a state of surveillance with elongated processes. During injury or neurodegenerative processes, microglial cells become activated; the activated state is mirrored by upregulation of translocator protein (TSPO) (*1,2*). PET with TSPO-specific ligands provides an in vivo technique to detect microglial activation (*3*).

^{11}C-(*R*)-PK11195 PET has been used for more than 2 decades. However, because of a low signal-to-background ratio and short half-life (20 min), second-generation TSPO markers have been developed. These include ^{18}F-FEPPA, ^{18}F-FEDAA1106, ^{11}C-vinpocetine, ^{11}C-DAC, ^{11}C-DAA1106, ^{11}C-N1-methyl-2-phenylindol-3-ylglyoxylamide, ^{11}C-CLINME, ^{11}C-DPA-713, ^{18}F-DPA-714, ^{18}F-PBR06, and ^{11}C-PBR28 (*4*). However, the results obtained by second-generation radioligands in preclinical models have not been consistently reproduced in humans (*5*). Their quantification in humans suffers from 3 confounding factors (*6*). The first factor is genetic: a single nucleotide polymorphism in the TSPO gene (rs6971) leads to an amino-acid substitution (A147T) and reduced binding affinity. The second factor is the disproportion between the high signal from the TSPO in the endothelial cells of the blood–brain barrier (BBB) and venous sinuses and the signal from the tissue, requiring appropriate kinetic correction (*7*). The third factor is the difficulty in obtaining accurate estimates of free plasma concentrations for proper quantification.

Flutriciclamide (^{18}F-GE180) has been identified as a promising TSPO tracer in preclinical models of stroke and lipopolysaccharide-induced central nervous system inflammation (*8,9*). Here we report the results of a study evaluating ^{18}F-GE180 PET in healthy human brains. We have investigated blood tracer concentrations, brain uptake, quantification of binding via tracer kinetic modeling, optimal scan length, and feasibility of generating parametric maps.

MATERIALS AND METHODS

Fifteen healthy controls (HCs) aged 50–85 y were recruited. Subjects who were high-affinity binders (HABs = 6) or mixed-affinity

Received Nov. 23, 2015; revision accepted May 10, 2016.
For correspondence or reprints contact: Paul Edison, Neurology Imaging Unit, Imperial College London, Hammersmith Hospital Campus, London, W12 0NN, U.K.
E-mail: paul.edison@imperial.ac.uk
*Contributed equally to this work.
Published online Jun. 3, 2016.
COPYRIGHT © 2016 by the Society of Nuclear Medicine and Molecular Imaging, Inc.

Downloaded from jnm.snmjournals.org by UCL Library Services on July 9, 2019. For personal use only.

binders (MABs = 4) proceeded to MRI and PET scans, whereas low-affinity binders (n = 5) were excluded. Details of recruitment, demography, and MRI acquisition are provided in the supplemental materials (available at http://jnm.snmjournals.org).

GE180 PET

^{18}F-GE180 was manufactured on the FASTlab (GE Healthcare) (*10*). All subjects received 185 MBq of ^{18}F-GE180 by bolus intravenous injection (in 20 s) immediately before the PET scan. The scan was acquired using a Biograph 6 PET/CT scanner (Siemens) (*11*). An initial CT was acquired for patient position and for attenuation correction of PET images. The tracer was then injected, and dynamic emission PET images were acquired over 210 min using predetermined time frames: 6 × 15, 3 × 60, 5 × 120, 5 × 300, and 14 × 600 s. Images were corrected for attenuation, random, and scattered emissions based on the 3-dimensional ordinary Poisson ordered-subset expectation maximization algorithm. Reconstruction of PET was performed using filtered backprojection.

Blood Data

Arterial whole-blood activity was continuously monitored for the first 15 min of the PET scan using the Allogg automated blood sampling system with real-time online blood sampling. Ten discrete arterial blood samples were taken at 5, 10, 15, 30, 60, 90, 120, 150, 180, and 210 min of the PET scan. The activity concentration was measured in both whole blood and plasma by a well-counter and was used to generate a plasma-to-blood ratio curve. The time course of activity in the plasma can be estimated with a sigmoidal fitting using the plasma-to-blood ratio model to the first 15 min of continuous whole-blood data.

Metabolites of ^{18}F-GE180 were measured by high-performance liquid chromatography analysis (*10*) using discrete blood samples. A 2-exponential linear model was used to describe the parent fraction of ^{18}F-GE180, which was applied to the plasma to generate the parent plasma input function. SUV was applied to both total blood and parent plasma with the formula:

$$\text{SUV} = \frac{^{18}\text{F-GE180 activity concentration (kBq/mL)}}{^{18}\text{F-GE180 injected dose (MBq)}/_{\text{body weight (kg)}}}.$$

Finally, the time delay (the arrival of the ^{18}F-GE180 bolus at the peripheral sampling site) was determined using MICK.exe (quantitative software for the PET analysis) and was performed using MATLAB 2014 (The MathWorks, USA) on a Windows platform.

Region-of-Interest (ROI) Analysis

Each subject underwent two 90-min PET scans with a 20-min break in between; the realignment approach was necessary to realign the second scan to the first scan. Head motions were corrected using the frame-by-frame realignment tools in statistical parametric mapping. On the basis of the visual resolution, the eighth frame (185–245 s) was selected as the reference frame for each time frame realigning to. An individualized object map in PET space was created with the following procedure: MRI was coregistered to the PET add image (60–90 min), a binary gray and white matter mask was created via segmentation, the probabilistic ROI atlas (*12*) in MNI space was transformed into native PET space, and a binary mask was applied to the ROI atlas to generate individual ROIs. Regional time–activity curves were generated by sampling the dynamic PET images with the individual ROIs for the following merging regions: frontal, temporal, parietal, and occipital lobes and whole brain. Additional sampling of the posterior cingulate, thalamus, brain stem, whole medial temporal lobe, hippocampus, and cerebellum was performed. The parahippocampus, anterior cingulate, and amygdala were sampled as additional ROIs using Analyze 11.0 (AnalyzeDirect). The SUV time–activity curve was generated for each ^{18}F-GE180 dynamic PET by dividing the ratio of ^{18}F-GE180–injected dose over body weight.

Kinetic Modeling

Parent plasma input function and dynamic PET were used to investigate the best kinetic model to compute ^{18}F-GE180 total volume of distribution (V_T) from time–activity curves with MICK software (Modeling-Input-function-Compartmental-Kinetics) and MATLAB. We evaluated 5 different kinetic models (supplemental materials). ^{18}F-GE180 tissue data were investigated with the reversible 1-tissue 2k (1TCM2k) model, the 2-tissue 4k (2TCM4k) model, and the irreversible 2-tissue 3k, for which k implies the rate constant for tracer for different kinetic compartments. As tracer binds to BBB endothelial cells, endothelia could significantly affect kinetic modeling (*7,13*); therefore, we also considered 1 tissue with extra vascular component (1TCM2k-1k) and 2-tissue with extra vascular component (2TCM4k-1k). The additional component describes the trapping of the tracer by the endothelial cells of blood vessels. The Akaike information criterion (AIC) (*14*) is a statistical measure to estimate the quality of fit of the predicted model against the actual data using different statistical models. In simple terms, the AIC values indicate the information lost when a candidate model is applied to estimate the real data, and the model with the smallest AIC value should be selected as the preferred model, as it indicates the best fit (*15*). To select the best model to quantify the tracer, AIC is calculated using the following formula:

$$\text{AIC} = \text{n} \times \ln(\text{wrss}) + 2\text{m},$$

where m denotes number of parameters, n equals the sum of degrees of freedom and number of parameters, and wrss denotes weighted residual sum of squares (*16*). The AIC fraction was also calculated by measuring the frequency of AIC preferences for each model across all subjects (*17*). AIC was calculated for the following brain regions: frontal, temporal, parietal, and occipital lobes; whole brain; posterior cingulate; thalamus; striatum; brain stem; medial temporal lobe; hippocampus; and cerebellum. Coefficient of variation (CV) was measured to assess dispersion and precision of parameters. We also evaluated the separation in average binding between HAB and MAB classes.

Graphical Analysis

Graphical analysis was applied to investigate the feasibility of generating parametric maps of ^{18}F-GE180. We used the Logan plot to generate pixel-wise parametric maps. Initially we calculated the optimal threshold time by linear fit, the tissue-to-plasma ratio against the time. ^{18}F-GE180 parametric maps were generated with the parent plasma input function and dynamic PET images using MICK parametric map software on MATLAB.

Optimization of Scan Length

The optimum scan duration was evaluated, measuring the percentage change of k (rate constants) and V_T, along with their CV at different time durations, calculated at 60, 75, 90, 150, 180, and 210 min. k_3 and k_4 indicate the rate constant of ^{18}F-GE180 in and out of the specific-bound compartment, whereas the k_3/k_4 ratio represents the specific binding of the tracer. Thus, the k_3/k_4 ratio was measured to investigate whether the binding potential of ^{18}F-GE180 was affected when the scanning time was reduced.

Statistical Analysis

Statistical analysis of groupwise differences between different kinetic models, different scan durations, and ROI V_T in different genetic groups was calculated in SPSS for Windows (version 22; SPSS). A P value of less than 0.05 was regarded as a statistical difference. The Pearson correlation was applied to measure the linear correlation

Downloaded from jnm.snmjournals.org by UCL Library Services on July 9, 2019. For personal use only.

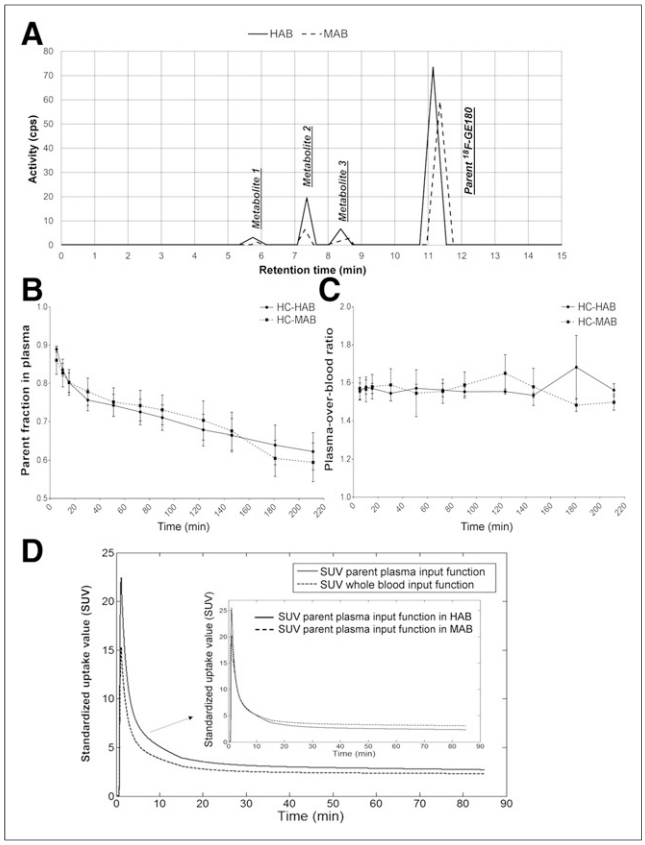

FIGURE 1. ^{18}F-GE180 blood data. (A) HPLC analysis for ^{18}F-GE180 at 15 min in HAB subject (solid line) and MAB subject (dashed line). (B) ^{18}F-GE180 parent fraction in arterial plasma. (C) Plasma-to-blood ratio in HABs (●) and MABs (■). (D) SUV for parent plasma and whole blood as group and parent plasma input function curve in either HAB or MAB cohorts.

between 2 groups of variables using SPSS. Repeated-measures ANOVA was applied to detect any overall differences between repeated measurements.

RESULTS

Parent Plasma Input

Consistent with the preclinical work (*8*), the radiochromatogram revealed 3 identifiable radiolabeled metabolites and a parent ^{18}F-GE180 in human plasma (Fig. 1A). The parent fraction of ^{18}F-GE180 gradually reduced from 90% to 60%. There was no group difference between HABs and MABs in metabolic rates and plasma-to-blood curve (Figs. 1B and 1C). The ^{18}F-GE180 activity concentration in plasma was 1.6-fold higher than in whole blood. No difference in parent plasma input function between HABs and MABs was found (Fig.1D).

Dynamic PET Image Time–Activity Curve

Because tracer concentrations are correlated with injected dose and individual weight, we measured SUV time–activity curve values at each time frame. The tracer activity concentration in the brain peaked at 125 s, with SUV at 1.5, and then quickly washed out and reached a plateau around 40 min. As a group, SUVs were significantly higher in HABs than MABs in the temporal lobe (P = 0.0001), thalamus (P = 0.0001), and striatum (P = 0.0002) (Fig. 2). The venous sinuses showed consistently highest tracer activity throughout the scan, whereas gray matter showed around 30% higher activity concentration than white matter.

Kinetic Modeling

Among 5 kinetic models, 2TCM4k showed the lowest AIC values in frontal (−59.6 ± 5.4), temporal (−46.4 ± 4.5), parietal (−58.6 ± 5.4), and occipital lobes (−54.3 ± 5.1) as a group (Fig. 3A). The 2TCM4k model also showed the highest AIC fraction (Fig. 3B). Although the 2TCM3k irreversible model demonstrated closer AIC values (<10% difference compared with the 2TCM4k model), the Ki (net influx constant), demonstrating the overall net rate of tracer uptake into tissue in the 2TCM3k model, showed poor precision with a high CV (104% ± 85%) whereas V_T in the reversible 2TCM4k model had a CV of 21% ± 13%. On the basis of the model curve fitting, 2TCM4k provided a good fit to ^{18}F-GE180 activity, supported by smallest weighted residual sum square and more random in residual's sequence (similar number of residuals above or below the model curve) using the Wald–Wolfowitz test. In summary, the 2TCM4k is the preferred method of analysis of ^{18}F-GE180 PET. The supplemental materials detail rate constants (K_1, k_2, k_3, and k_4), blood volume, and V_T, applying the 2TCM4k model in HABs and MABs, which showed good precision of parameter estimation.

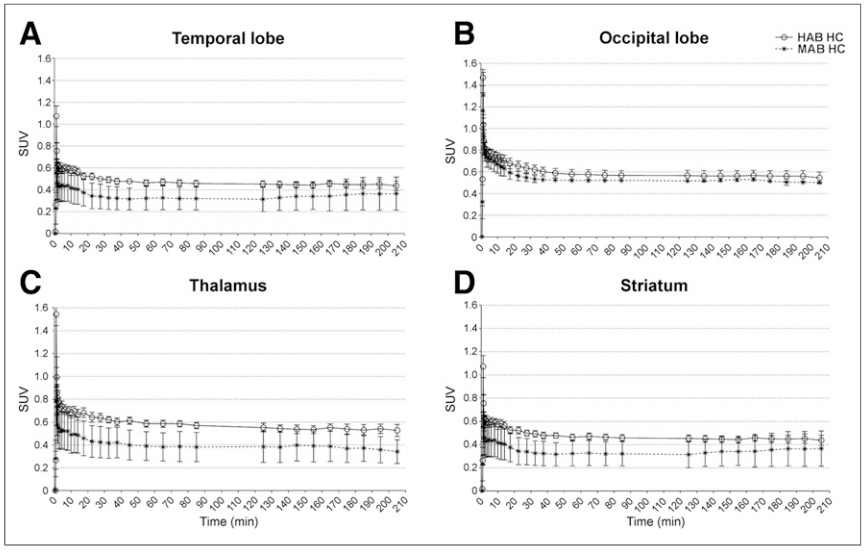

FIGURE 2. SUV corrected time–activity curves of ^{18}F-GE180 in temporal and occipital lobes (A and B), thalamus (C), and striatum (D) for HABs (○) and MABs (*).

V_T

As a group, 10 HCs had low mean V_T in the whole brain but slightly higher in temporal the lobe, occipital lobe, and thalamus (Fig. 4). The thalamus, parahippocampus (47%, P = 0.04), and cerebellum showed significantly higher mean V_T values in HABs than in MABs (Table 1).

Scan Length

The 210-min data were excluded because variance was high toward the end of the scan. Repeated ANOVA did not show difference in the absolute V_T when the scan duration was reduced. In this study, the group

Downloaded from jnm.snmjournals.org by UCL Library Services on July 9, 2019. For personal use only.

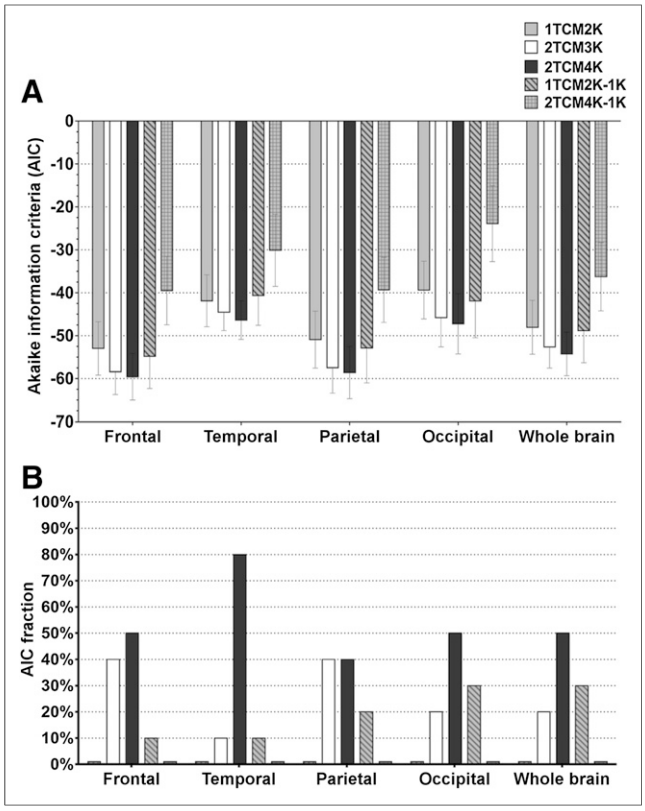

FIGURE 3. Kinetic model selection. (A) AIC values for 5 models in frontal, temporal, parietal, and occipital lobes and whole brain. (B) Graph with AIC fraction, revealing frequency of AIC preferences for each model across all subjects.

mean of k_3/k_4 ratio (HAB = 0.52 and MAB = 0.34) was calculated to evaluate the results among different scan lengths, showing no differences with scan length reduction from 180 to 90 min. When the scan length was further reduced to 75 min, the k_3/k_4 ratio remained the same as with the 90-min data, but 4 individual subjects showed a 14% reduction in k_3/k_4 ratio. Compared with 90-min scans, 60-min scans showed a 51% reduction in k_3/k_4 ratio as a group. These data suggest that for this cohort the optimal scan duration is 90 min.

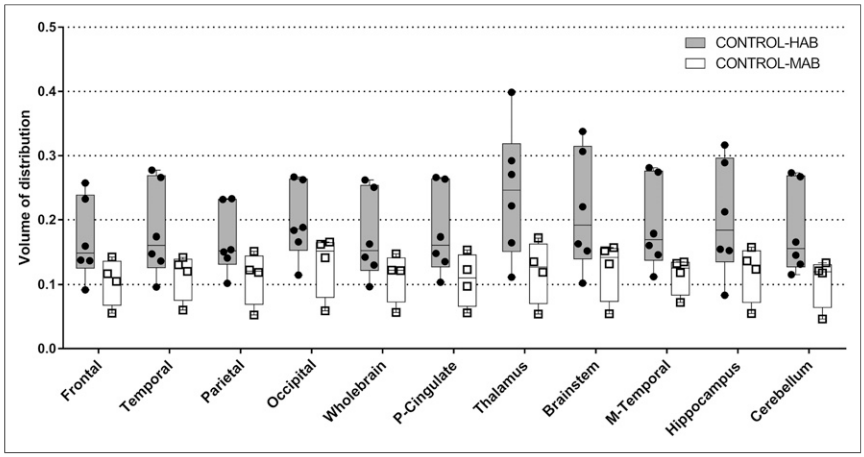

FIGURE 4. ^{18}F-GE180 regional V_T in 2TCM4k model. Regional V_T with application of 2TCM4k model in 11 ROI regions. Circle with black bar represents HABs, and square with white bar represents MABs. M = medial; P = posterior.

Logan

Kinetic modeling suggested that ^{18}F-GE180 has a reversible feature, therefore we applied Logan graphical analysis (*18*) to generate parametric maps. On the basis of linear fit of the whole brain and the appropriate weight for different time points, dynamic data from 20 to 90 min (8 data points) were selected to generate a Logan straight line (slope = 0.147 ± 0.06 and intercept = −1,623 ± 387) for parametric maps (Fig. 5). The Logan V_T values (supplemental materials) were correlated with 2TCM4k V_T values, with a strong correlation in 4 cortices and hippocampus in both HABs ($P < 0.0001$) and MABs ($P < 0.0001$) (Fig. 6). The HABs showed generally higher Logan V_T values than MABs; however, there were no statistically significant differences in this small sample.

DISCUSSION

To our knowledge, this is the first study evaluating different approaches for PET modeling of the third-generation TSPO tracer ^{18}F-GE180 in older healthy subjects, establishing the optimum scanning time in this study population. There was consistently higher ^{18}F-GE180 activity in plasma than in whole blood, but brain V_T values generated from plasma input functions were low (~0.16). Data were acquired for 210 min after injection of ^{18}F-GE180, and 5 different kinetic models were evaluated in this study. The ^{18}F-GE180 V_T remained unchanged when the scan length was reduced to 90 min, but changes were observed when the scan length was reduced to 75 and 60 min, suggesting that 90 min might be the minimal scan time for ^{18}F-GE180 PET. The 2TCM4k model demonstrated the lowest AIC and CV among the 5 kinetic models, suggesting that the 2TCM4k model could be the best model to estimate ^{18}F-GE180 uptake. Compared with the 2TCM4k model, Logan graphical analysis allows us to create parametric maps and to estimate V_T at the voxel level. Logan V_T was highly correlated with 2TCM4k V_T in all cortices, indicating that the Logan graphical analysis can be used to create unbiased parametric V_T maps for ^{18}F-GE180.

Consistent with a preclinical study (*8*), high-performance liquid chromatography revealed 3 separate ^{18}F-GE180 plasma metabolites, with a similar profile in HAB and MAB and no significant differences between HABs and MABs in plasma-to-blood ratios. The plasma-to-blood ratio for tracers crossing the BBB by passive diffusion is close to unity at the beginning of PET. ^{18}F-GE180 showed a relatively high plasma-to-blood ratio of 1.55, indicating higher concentration in plasma than red blood cells. A persistently high plasma-to-blood ratio throughout the scan reflects poor membrane penetration of ^{18}F-GE180 across red cell membranes. In vitro assays of plasma protein binding of ^{18}F-GE180 in human samples showed a relatively high percentage (97.4%) plasma protein binding, which was also seen with other TSPO tracers.

Preclinical animal models showed that ^{18}F-GE180 crosses the BBB readily. In humans, ^{18}F-GE180 demonstrated a relatively low V_T in the brain, possibly because of low availability of the GE180 due to significant plasma protein binding, low BBB permeability, or clearance by efflux pumps.

Downloaded from jnm.snmjournals.org by UCL Library Services on July 9, 2019. For personal use only.

TABLE 1
Regional V_T for ^{18}F-GE180 Applied 2TCM4k Model in All HCs, HABs, and MABs

^{18}F-GE180 2TCM4K	FL	TL	PL	OL	WB	P-cing	Thalamus	Brain stem	Striatum	MTL	Hippo	CB
All subjects												
Mean	0.15	0.16	0.15	0.17	0.15	0.16	0.20	0.19	0.15	0.17	0.17	0.15
SD	0.06	0.07	0.05	0.06	0.06	0.06	0.09	0.09	0.06	0.06	0.08	0.07
TSPO genetic subgroup												
HAB												
Mean	0.17	0.18	0.17	0.20	0.17	0.18	0.24	0.21	0.17	0.19	0.20	0.18
SD	0.06	0.07	0.05	0.06	0.07	0.06	0.09	0.09	0.05	0.07	0.08	0.07
MAB												
Mean	0.12	0.13	0.12	0.14	0.12	0.12	0.14	0.16	0.10	0.13	0.13	0.11
SD	0.05	0.05	0.05	0.05	0.05	0.05	0.06	0.09	0.05	0.05	0.06	0.05
HAB vs. MAB												
T test	0.11	0.09	0.12	0.06	0.11	0.07	0.04*	0.18	0.07	0.06	0.09	0.05*
Increase	39%	45%	36%	45%	40%	49%	73%	36%	64%	50%	51%	63%

*$P < 0.05$.
FL = frontal lobe; TL = temporal lobe; PL = parietal lobe; OL = occipital lobe; WB = whole brain; P-cing = posterior cingulate; MTL = medial temporal lobe; Hippo = hippocampus; CB = cerebellum.

Despite the fact that species differences have been observed in the BBB structure (*19*) and other novel brain PET tracers (*20*), the significant difference observed between human and preclinical models in ^{18}F-GE180 could be primarily due to a significantly higher binding to plasma protein in humans.

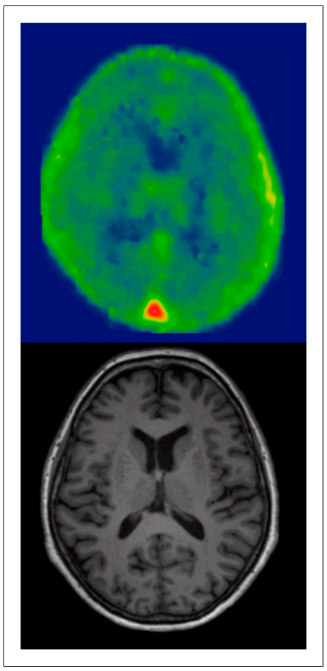

FIGURE 5. Individual ^{18}F-GE180 Logan parametric maps in transverse view are demonstrated with corresponding MR image.

^{18}F-GE180 preclinical studies demonstrated that, in rats, there is a clear regional differentiation of high-TSPO-expressing regions (olfactory bulbs) compared with low-TSPO-expressing regions (striatum) (*21*). In this study, 5 subjects (1 MAB and 4 HABs) revealed lowest uptake in the striatum: 3 (MABs) showed lowest uptake in the cerebellum and 2 (HABs) showed a more generalized distribution of TSPO expression. This inconsistent pattern suggests that a single predefined reference region for nonspecific binding may not be appropriate for ^{18}F-GE180 in humans in this age group.

Because TSPO expression is low in the healthy brain, the ^{18}F-GE180 V_T values were relatively small in all ROI regions (range, 0.15–0.20). A higher signal in the thalamus than other regions was found, consistent with previous ^{11}C-(*R*)-PK11195 studies (*22*). However, V_T values for ^{18}F-GE180 suggest that tracer brain uptake is relatively low compared with other TSPO PET radioligands, though the impact of this radioligand as a microglial imaging marker cannot be determined until we have results in specific disease conditions. The significant inverse correlation between the ^{18}F-GE180 input function and the tracer uptake in the brain reflects the higher uptake to plasma proteins in humans than animal models.

Interestingly, the significant inverse correlation between ^{18}F-GE180 input function and V_T in the brain for each binding class separately, with a correlation coefficient greater than 0.9, indicates that whole-brain V_T can be almost entirely predicted by plasma levels within each binding class. As we were unable to estimate plasma free fractions reliably, the fluctuations in estimated V_T may be due to fluctuations in free plasma fractions across subjects. Indeed, higher plasma protein binding would result in higher plasma counts and lower V_T. This observation replicates similar observations in other TSPO tracers (*13,23*). Identification of an optimal reference method would allow us to further refine the analysis methods without the arterial input.

Most second-generation TSPO tracers, such as ^{11}C-PBR28 and ^{11}C-PBR111, demonstrated an association with the TSPO genotype, revealing a 30% higher uptake in the whole brain of HABs than MABs. In this study, there was a 30%–40% higher uptake in HABs, reaching significance in the thalamus, parahippocampus, and cerebellum. Nevertheless, there was some overlap between subjects; moreover, the study cohort was also small. Compared with some second-generation TSPO tracers, ^{18}F-GE180 may be less sensitive to the TSPO binding affinity status and may behave more like ^{11}C-(*R*)-PK11195. One could argue, some of the variability seen in the MABs and HABs could be due to test–retest

Downloaded from jnm.snmjournals.org by UCL Library Services on July 9, 2019. For personal use only.

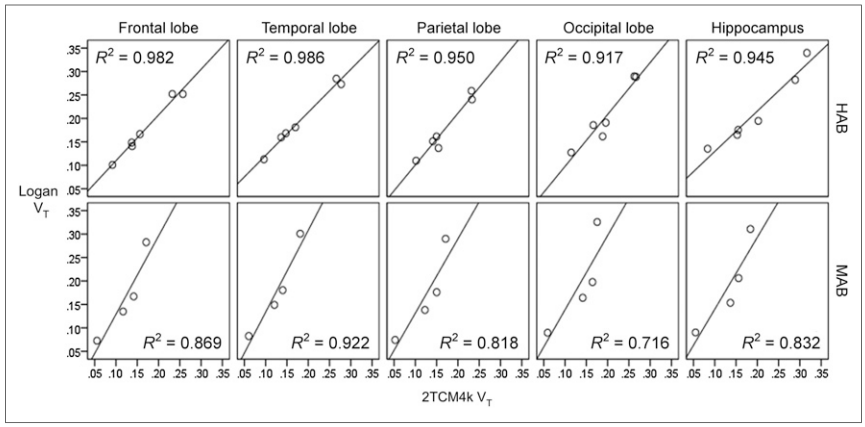

FIGURE 6. V_T in 2-tissue-reversible model and Logan parametric map demonstrate similar V_T results with strong Pearson correlation in 4 cortices and hippocampus in both HABs ($P < 0.0001$) and MABs ($P < 0.0001$).

variability, which we are evaluating. The high correlation between Logan V_T and 2TCM4k V_T suggests that Logan parametric mapping could be used to generate pixelwise parametric V_T maps. Because Logan generally underestimates the V_T (*24*), there was no statistically significant difference between HAB and MAB, potentially because of the small numbers in this pilot study. Additionally, consistently with V_T results, the Logan V_T parametric maps demonstrated heterogeneous distribution of ^{18}F-GE180 uptake in the HCs. This heterogeneity was observed in both HAB and MAB subgroups and was consistent with 2TCM4k model.

Although one of the limitations of this study is the small sample size, this pilot study provides the first insight into the performance of ^{18}F-GE180 in the normal human brain and information about the parent plasma input function. Another limitation is the exclusion of the low-affinity binders from the study, and our laboratory is recruiting more participants to evaluate this tracer further. The low expression of TSPO in the normal brain could be another limitation of this study evaluating only HCs. However, these scans were obtained with an arterial input function and an extensive scanning time of 210 min, providing significant information about the tracer kinetics and modeling of this novel TSPO tracer for future use.

CONCLUSION

This pilot study provides preliminary brain uptake kinetics of the novel TSPO tracer ^{18}F-GE180 in HCs. We have demonstrated for the first time, to our knowledge, that ^{18}F-GE180 shows uptake into the brain of HCs and that the tracer V_T could be effectively modeled using 2TCM4k and Logan graphical models to quantify the TSPO binding in the human brain. The plasma-to-blood ratio and the rate of metabolism and input functions were not different between HAB and MAB subjects. We have also demonstrated that 90 min is the optimal scan duration, providing enough information to generate the precise and accurate estimates of V_T. Semiquantitative SUV analysis for tracer uptake demonstrated a good correlation with kinetic modeling V_T values. Logan graphical analysis with arterial input function enables us to generate ^{18}F-GE180 parametric maps for voxelwise analyses.

DISCLOSURE

The costs of publication of this article were defrayed in part by the payment of page charges. Therefore, and solely to indicate this fact, this article is hereby marked "advertisement" in accordance with 18 USC section 1734. This work received financial support from Alzheimer's Research U.K., GE Healthcare, and the National Institute for Health Research. Dr. Paul Edison was funded by the Higher Education Funding Council for England and received grants from Alzheimer's Research, U.K., Alzheimer's Drug Discovery Foundation, Alzheimer's Society, U.K., Novo Nordisk, Piramal Life Science, and GE Healthcare. Calsolaro Valeria was funded by the Alzheimer's Research U.K. fellowship. Drs. William Trigg and Christopher Buckley were funded by GE Healthcare. Prof. David J. Brooks received research grants from the Medical Research Council and Alzheimer's Research Trust, during the conduct of the study, as well as other grants from GE Healthcare; personal fees from AstraZeneca, Cytox, Shire, Novartis, GSK (Holland), Navidea, UCB, and Acadia; and grants from the Michael J. Fox Foundation and European Commission, outside the submitted work. No other potential conflict of interest relevant to this article was reported.

ACKNOWLEDGMENTS

We thank GE Healthcare for providing the radiotracers and the Imperial College Clinical Imaging Facility for providing MRI and PET imaging facilities. We thank Dr. Albert Busza, Andy Blyth, Stephanie McDevitt, Neva Patel, and Gokul Kolipaka for ^{18}F-GE180 scanning.

REFERENCES

1. Lavisse S, Guillermier M, Herard AS, et al. Reactive astrocytes overexpress TSPO and are detected by TSPO positron emission tomography imaging. *J Neurosci.* 2012;32:10809–10818.
2. Gatliff J, Campanella M. TSPO: kaleidoscopic 18-kDa amid biochemical pharmacology, control and targeting of mitochondria. *Biochem J.* 2016;473:107–121.
3. Ching AS, Kuhnast B, Damont A, Roeda D, Tavitian B, Dolle F. Current paradigm of the 18-kDa translocator protein (TSPO) as a molecular target for PET imaging in neuroinflammation and neurodegenerative diseases. *Insights Imaging.* 2012;3:111–119.
4. Chauveau F, Boutin H, Van Camp N, Dolle F, Tavitian B. Nuclear imaging of neuroinflammation: a comprehensive review of [^{11}C]PK11195 challengers. *Eur J Nucl Med Mol Imaging.* 2008;35:2304–2319.
5. Rahmim A, Qi J, Sossi V. Resolution modeling in PET imaging: theory, practice, benefits, and pitfalls. *Med Phys.* 2013;40:064301.
6. Turkheimer FE, Rizzo G, Bloomfield PS, et al. The methodology of TSPO imaging with positron emission tomography. *Biochem Soc Trans.* 2015;43:586–592.
7. Rizzo G, Veronese M, Tonietto M, Zanotti-Fregonara P, Turkheimer FE, Bertoldo A. Kinetic modeling without accounting for the vascular component impairs the quantification of [^{11}C]PBR28 brain PET data. *J Cereb Blood Flow Metab.* 2014;34:1060–1069.
8. Boutin H, Murray K, Pradillo J, et al. ^{18}F-GE-180: a novel TSPO radiotracer compared to ^{11}C-R-PK11195 in a preclinical model of stroke. *Eur J Nucl Med Mol Imaging.* 2015;42:503–511.
9. Dickens AM, Vainio S, Marjamaki P, et al. Detection of microglial activation in an acute model of neuroinflammation using PET and radiotracers ^{11}C-(R)-PK11195 and ^{18}F-GE-180. *J Nucl Med.* 2014;55:466–472.

Downloaded from jnm.snmjournals.org by UCL Library Services on July 9, 2019. For personal use only.

10. Wickstrøm T, Clarke A, Gausemel I, et al. The development of an automated and GMP compliant FASTlab synthesis of [^{18}F]GE-180; a radiotracer for imaging translocator protein (TSPO). *J Labelled Comp Radiopharm.* 2014;57:42–48.
11. Poon JK, Dahlbom ML, Casey ME, Qi J, Cherry SR, Badawi RD. Validation of the SimSET simulation package for modeling the Siemens Biograph mCT PET scanner. *Phys Med Biol.* 2015;60:N35–N45.
12. Hammers A, Chen CH, Lemieux L, et al. Statistical neuroanatomy of the human inferior frontal gyrus and probabilistic atlas in a standard stereotaxic space. *Hum Brain Mapp.* 2007;28:34–48.
13. Guo Q, Owen DR, Rabiner EA, Turkheimer FE, Gunn RN. Identifying improved TSPO PET imaging probes through biomathematics: the impact of multiple TSPO binding sites in vivo. *Neuroimage.* 2012;60:902–910.
14. Aho K, Derryberry D, Peterson T. Model selection for ecologists: the worldviews of AIC and BIC. *Ecology.* 2014;95:631–636.
15. Akaike H. Information theory and an extension of the maximum likelihood principle. In: *Selected Papers of Hirotugu Akaike*. New York, NY: Springer; 1998:199–213.
16. Turkheimer FE, Hinz R, Cunningham VJ. On the undecidability among kinetic models: from model selection to model averaging. *J Cereb Blood Flow Metab.* 2003;23:490–498.
17. Mansor S, Boellaard R, Froklage FE, et al. Quantification of dynamic ^{11}C-phenytoin PET studies. *J Nucl Med.* 2015;56:1372–1377.
18. Logan J. Graphical analysis of PET data applied to reversible and irreversible tracers. *Nucl Med Biol.* 2000;27:661–670.
19. Syvänen S, Lindhe O, Palner M, et al. Species differences in blood-brain barrier transport of three positron emission tomography radioligands with emphasis on P-glycoprotein transport. *Drug Metab Dispos.* 2009;37:635–643.
20. Alstrup AK, Landau AM, Holden JE, et al. Effects of anesthesia and species on the uptake or binding of radioligands in vivo in the Gottingen minipig. *Biomed Res Int.* 2013;2013:808713–808719.
21. Wadsworth H, Jones PA, Chau WF, et al. [^{18}F]GE-180: a novel fluorine-18 labelled PET tracer for imaging translocator protein 18 kDa (TSPO). *Bioorg Med Chem Lett.* 2012;22:1308–1313.
22. Doble A, Malgouris C, Daniel M, et al. Labelling of peripheral-type benzodiazepine binding sites in human brain with [^{3}H]PK 11195: anatomical and subcellular distribution. *Brain Res Bull.* 1987;18:49–61.
23. Endres CJ, Pomper MG, James M, et al. Initial evaluation of ^{11}C-DPA-713, a novel TSPO PET ligand, in humans. *J Nucl Med.* 2009;50:1276–1282.
24. Slifstein M, Laruelle M. Effects of statistical noise on graphic analysis of PET neuroreceptor studies. *J Nucl Med.* 2000;41:2083–2088.

Downloaded from jnm.snmjournals.org by UCL Library Services on July 9, 2019. For personal use only.

JNM The Journal of NUCLEAR MEDICINE

Flutriciclamide (^{18}F-GE180) PET: First-in-Human PET Study of Novel Third-Generation In Vivo Marker of Human Translocator Protein

Zhen Fan, Valeria Calsolaro, Rebecca A. Atkinson, Grazia D. Femminella, Adam Waldman, Christopher Buckley, William Trigg, David J. Brooks, Rainer Hinz and Paul Edison

J Nucl Med. 2016;57:1753-1759.
Published online: June 3, 2016.
Doi: 10.2967/jnumed.115.169078

This article and updated information are available at:
http://jnm.snmjournals.org/content/57/11/1753

Information about reproducing figures, tables, or other portions of this article can be found online at:
http://jnm.snmjournals.org/site/misc/permission.xhtml

Information about subscriptions to JNM can be found at:
http://jnm.snmjournals.org/site/subscriptions/online.xhtml

The Journal of Nuclear Medicine is published monthly.
SNMMI | Society of Nuclear Medicine and Molecular Imaging
1850 Samuel Morse Drive, Reston, VA 20190.
(Print ISSN: 0161-5505, Online ISSN: 2159-662X)

© Copyright 2016 SNMMI; all rights reserved.

SNMMI SOCIETY OF NUCLEAR MEDICINE AND MOLECULAR IMAGING